Obesity-Induced Endothelial Dysfunction Is Prevented by Deficiency of P-Selectin Glycoprotein Ligand-1

Hui Wang,[1] Wei Luo,[1] Jintao Wang,[1] Chiao Guo,[1] Xiaohong Wang,[1] Stephanie L. Wolffe,[1] Peter F. Bodary,[2] and Daniel T. Eitzman[1]

Endothelial dysfunction precedes atherosclerosis and represents an important link between obesity and cardiovascular events. Strategies designed to prevent endothelial dysfunction may therefore reduce the cardiovascular complications triggered by obesity. We tested the hypothesis that deficiency of P-selectin glycoprotein ligand-1 (Psgl-1) would improve the endothelial dysfunction associated with obesity. Psgl-1-deficient (*Psgl-1*$^{-/-}$) and wild-type (*Psgl-1*$^{+/+}$) mice were fed standard chow or a high-fat, high-sucrose diet (diet-induced obesity [DIO]) for 10 weeks. DIO increased mesenteric perivascular adipose tissue (mPVAT) macrophage content and vascular oxidative stress in *Psgl-1*$^{+/+}$ mice but not in *Psgl-1*$^{-/-}$ mice. Pressure myography using mesenteric arteries demonstrated that relaxation responses to acetylcholine were significantly impaired in DIO *Psgl-1*$^{+/+}$ mice, whereas DIO *Psgl-1*$^{-/-}$ mice were protected from endothelial dysfunction with similar relaxation responses to *Psgl-1*$^{+/+}$ or *Psgl-1*$^{-/-}$ mice fed standard chow. The superoxide scavenger 4-hydroxy-2,2,6,6-tetramethylpiperidinyloxy (TEMPOL) partially recovered impaired endothelial function induced by DIO. A neutralizing Psgl-1 antibody was also effective in preventing endothelial dysfunction and reducing mPVAT macrophage content induced by DIO. These results indicate that obesity in mice leads to PVAT inflammation and endothelial dysfunction that is prevented by Psgl-1 deficiency. Psgl-1 inhibition may be a useful treatment strategy for targeting vascular disease associated with obesity. ***Diabetes*** **61:3219–3227, 2012**

Obesity is epidemic in the United States and is associated with increased risk for cardiovascular complications (1). Excess visceral adipose tissue may be the primary driver of the vascular risk associated with obesity because visceral fat is strongly associated with a chronic, low-grade inflammatory state characterized by increased macrophage activity in adipose tissue (2,3). The mechanism(s) by which obesity promotes vascular disease is unclear, but endothelial dysfunction has been demonstrated even in children with obesity (4,5). Endothelial dysfunction due to impairment of nitric oxide (NO) activity represents an early stage of many cardiovascular diseases (6).

P-selectin glycoprotein ligand-1 (Psgl-1) is the primary leukocyte ligand for P-selectin (P-sel) and an important ligand for E-selectin (E-sel) (7). Psgl-1 deficiency has been shown to reduce leukocyte-endothelial interactions in obesity and to reduce macrophage accumulation in gonadal fat pads (8). The purpose of this study was to determine the effect of Psgl-1 deficiency on endothelial dysfunction associated with obesity.

From the [1]Department of Internal Medicine, Cardiovascular Research Center, University of Michigan, Ann Arbor, Michigan; and the [2]Department of Kinesiology, University of Michigan, Ann Arbor, Michigan.
Corresponding author: Daniel T. Eitzman, deitzman@umich.edu.
Received 13 February 2012 and accepted 13 June 2012.
DOI: 10.2337/db12-0162

See accompanying commentary, p. 3070.

RESEARCH DESIGN AND METHODS

Animals. Male C57BL6/J and *Psgl-1*$^{-/-}$ mice were originally purchased from The Jackson Laboratory (Bar Harbor, ME). *Psgl-1*$^{-/-}$ were backcrossed to the C57BL6/J strain >16 generations before use in these experiments. Mice were fed a standard laboratory rodent diet (No. 5001, TestDiet, Richmond, IN) or a high-fat, high-sucrose diet (HFD; D12451, Research Diets Inc, New Brunswick, NJ) and tap water ad libitum in a temperature-controlled room with a 12:12-h light/dark cycle. HFD was given for 10 weeks, beginning at age 8 weeks.

At age 18 weeks, blood pressure (BP) was measured in nonanesthetized mice by tail plethysmography using the BP-2000 Blood Pressure Analysis System (Visitech System, Apex, NC). All animal use protocols complied with the *Principle of Laboratory and Animal Care* established by the National Society for Medical Research and were approved by the University of Michigan Committee on Use of and Care of Animals.

Plasma measurements. Plasma samples were collected via ventricular puncture at time of euthanasia. Commercially available enzyme-linked immunosorbent assay (ELISA) kits were used to measure plasma soluble P-selectin (sP-sel), soluble E-selectin (sE-sel), monocyte chemoattractant protein-1 (MCP-1), leptin (R&D Systems, Minneapolis, MN), adiponectin (ALPCO Diagnostics, Salem, NH), and fasting insulin levels (Crystal Chemical Inc., Wakefield, MA) according to manufacturers' instructions. Overnight fasting blood glucose levels were measured using an Ascensia Contour Blood Glucose Meter and Ascensia Contour test strips (Bayer Healthcare LLC, Tarrytown, NY). Insulin resistance was determined using homeostasis model assessment-estimated insulin resistance (HOMA-IR) index by HOMA-IR equation: [HOMA-IR = fasting insulin (μIU/mL) × fasting glucose (mmol/L)/22.5] (9).

Real-time PCR. RNA from mouse mesenteric arteries was isolated using a QIAGEN RNeasy Mini Kit (QIAGEN Inc., Valencia, CA). RNA from 100 mg mesenteric perivascular adipose tissue (mPVAT) surrounding mesenteric arteries was isolated using QIAzol Lysis Reagent and QIAGEN RNeasy Mini Kit. The primer sets for specific amplification of interleukin-6 (IL-6), MCP-1, Psgl-1, leptin, and glyceraldehyde-3-phosphate dehydrogenase (GAPDH) were purchased from Applied Biosystems (Carlsbad, CA). Real-time PCR was performed using an ABI Prism 7000 Sequence Detection System (Applied Biosystems), with 100 ng RNA and 1 μL primer used per reaction. Results were analyzed using 7000 System SDS Software and the $2^{-\Delta\Delta CT}$ method (10) and were presented as fold-change of transcripts for target normalized to internal control (GAPDH).

Immunohistochemistry. The mPVAT surrounding mesenteric arteries was collected and fixed in zinc formalin. Macrophages in paraffin-embedded fat sections were identified with a rat anti-mouse Mac-3 monoclonal antibody (1:100; BD Biosciences, San Jose, CA), followed by detection with biotin-conjugated secondary goat anti-rat IgG (1:100; Accurate Chemical & Scientific Corp., Westbury, NY). Stained cells were counted manually from four randomly chosen fields in each section using Image-Pro software (Media Cybernetics, Inc., Bethesda, MD) and expressed as a percentage of total cells per field.

Vascular superoxide fluorescence microphotography. Vascular superoxide was detected using dihydroethidium (DHE) staining. Briefly, unfixed segments of mesenteric arteries were dissected in cold physiologic salt solution (PSS) containing (in mmol/L): NaCl, 120; KCl, 4.7; $MgSO_4$, 1.18; $CaCl_2$, 2.5; KH_2PO_4, 1.18; $NaHCO_3$, 25; glucose, 5.5; and EDTA, 0.026 (at pH 7.4). Surrounding tissues and intravascular blood were removed. The vessels were frozen in optimal cutting temperature compound and transverse sections (10 μm) were produced using a cryostat. Sections were incubated in a 37°C incubator for 30 min with 2 μmol/L DHE (Invitrogen, Carlsbad, CA). Images were obtained with a Leica laser scanning confocal microscope with an

excitation wavelength of 488 nm and emission wavelength of 597 to 610 nm. The intensity of fluorescence signal was quantified as arbitrary units using Image J software (National Institutes of Health, Bethesda, MD).

Immunoblotting. Mesenteric arteries were homogenized and lysed in E-PER lysis buffer (Thermo Scientific, Inc., Rockford, IL) supplemented with protease inhibitor cocktail (Roche, Branchburg, NJ). Protein concentration was assessed using BCA Protein Assay Kit (Thermo Scientific, Inc.), and equal amounts of protein were resolved by SDS-PAGE and then transferred to polyvinylidene fluoride membranes by electroblotting. Nitrotyrosine expression was detected using a mouse anti-mouse nitrotyrosine monoclonal antibody (Abcam, Cambridge, MA).

Functional and mechanical studies of mesenteric and carotid arteries. Mice were killed with intraperitoneal pentobarbital (80 mg/kg), and a segment of small intestine with attached mesentery was removed and placed into a silastic-elastomer–lined petri dish filled with cold PSS equilibrated with 5% CO_2 and 95% O_2. The second-order branches of mesenteric artery were dissected, and surrounding fat and connective tissue were cleared. Vessel segments 2–3 mm in length were mounted onto glass cannulae of a pressure myograph (Living Systems Instrumentation, Burlington, VT). Cannulae were adjusted to the axial direction of the vessel until the vessel walls were parallel without any stretch. Vessels were equilibrated in PSS at 37°C for 60 min at 45 mmHg intraluminal pressure. The real-time dimension of the vessel wall was detected and analyzed by a video dimension analyzer (Living Systems).

Vascular reactivity was tested under no-flow conditions. After equilibration, vascular viability was tested using extraluminal applied norepinephrine (NE; Sigma, St. Louis, MO) 10^{-5} mol/L plus KCl 125 mmol/L. The vessels were considered viable when the constriction of the luminal area exceeded 60%. After washing, vascular contraction was assessed by measuring constriction in response to cumulatively applied NE (10^{-8} to 10^{-4} mol/L).

After washing and equilibration, endothelium-dependent relaxation was assessed by measuring the dilatory response to acetylcholine (Ach; 10^{-9} to 10^{-4} mol/L; Sigma) in NE (10^{-5} mol/L) precontracted vessels. To determine the role of superoxide, Ach-induced vasorelaxation was examined after vessels were incubated for 30 min in 1 mmol/L TEMPOL (Sigma), a superoxide scavenger. To evaluate NO bioavailability, Ach-induced vessel relaxation was assessed after vessels were incubated for 20 min with the NO synthase inhibitor Nω-nitro-L-arginine methyl ester (L-NAME, 10^{-4} mol/L). Endothelium-independent relaxation was assessed by extraluminally applied sodium nitroprusside (SNP, 10^{-9} to 10^{-3} mol/L; Sigma) on the same vessel precontracted with NE (10^{-5} mol/L).

After the functional analyses, the mesenteric artery was incubated in Ca^{2+}-free PSS for 20 min. Then vascular wall thickness and lumen diameter were measured at 45 mmHg intraluminal pressure. Media cross sectional area (CSA) was calculated by subtraction of internal CSA from external CSA with the following equation: [CSA = $(\pi/4)(De^2 - Di^2)$], where *De* and *Di* were external and internal lumen diameters respectively. The media-to-lumen ratio was calculated by wall thickness/by lumen diameter.

For functional studies of carotid arteries, a segment of right common carotid artery was dissected and mounted onto pressure myograph. Vessels were equilibrated in PSS at 37°C for 60 min with 80 mmHg intraluminal pressure, then the vasoconstriction and vasorelaxation responses to phenylephrine or Ach (Sigma) were performed.

Fat incubation studies of mesenteric arteries. The mPVAT was collected from DIO *Psgl-1*$^{+/+}$ or DIO *Psgl-1*$^{-/-}$ mice. mPVAT (0.4 g) was homogenized in 4 mL diethyl maleic acid ester culture medium (Sigma) and centrifuged at 20,000*g* at 4°C for 30 min to obtain clear supernatant. The mesenteric artery collected from standard chow-fed *Psgl-1*$^{+/+}$ mice was mounted onto a pressure myograph and 500 μL fat supernatant was added to the myograph chamber for incubation. After incubation for 40 min, vascular response to NE, Ach, or SNP were assessed.

Antibody injections to animals. For antibody injection experiments, C57BL6/J mice were fed an HFD for 10 weeks beginning at age 8 weeks. After 5 weeks of the HFD, a rat anti-mouse Psgl-1 antibody 4RA10 or isotype control rat IgG_1 k (100 μg in 200 μL PBS; BD Biosciences, San Jose, CA) was injected intraperitoneally once a week for 5 weeks. Vascular function of mesenteric arteries was examined using the pressure myograph.

Statistical analysis. All data are presented as mean ± SE. Statistical analysis was done using GraphPad Prism software (GraphPad, La Jolla, CA). Results were analyzed using the unpaired *t* test for comparison between two groups. For multiple comparisons, results were analyzed using one-way or two-way ANOVA, followed by Tukey or Bonferroni post-test analysis. Probability values of $P < 0.05$ were considered statistically significant.

RESULTS

Metabolic parameters. Body weight, gonadal fat pad weight, mesenteric perivascular fat weight, and fasting blood glucose levels were elevated after 10 weeks of DIO compared with mice fed the standard diet, irrespective of genotype (n = 5–7 per group; Table 1). Body weight was similar between DIO *Psgl-1*$^{+/+}$ mice and DIO *Psgl-1*$^{-/-}$ mice ($P > 0.05$). Plasma free fatty acid (FFA) levels in DIO *Psgl-1*$^{+/+}$ mice were significantly elevated compared with other groups (Table 1). Fasting plasma insulin levels and systolic BP levels were similar between the groups, irrespective of diet and genotype (n = 5–7 per group) (Table 1). The HOMA-IR was significantly increased in DIO *Psgl-1*$^{+/+}$ mice compared with standard chow–fed *Psgl-1*$^{+/+}$ and *Psgl-1*$^{-/-}$ mice (Table 1). To verify the reliability of BP measurement using tail cuff, a positive control was performed using NE (0.2 mg/kg) injection subcutaneously. After the NE injection, the BP increased to 159.1 ± 6.3 mmHg compared with 112.0 ± 5.1 mmHg in a 0.9% NaCl-injected group (n = 3 per group, $P < 0.01$).

Circulating levels of sP-sel, sE-sel, MCP-1, and leptin. To determine the effect of DIO and Psgl-1 deficiency on a panel of circulating biomarkers, the levels of sP-sel, sE-sel, MCP-1, and leptin were measured from *Psgl-1*$^{+/+}$, DIO *Psgl-1*$^{+/+}$, *Psgl-1*$^{-/-}$, and DIO *Psgl-1*$^{-/-}$ mice. The levels of sP-sel and sE-sel in mice fed standard chow were significantly reduced in *Psgl-1*$^{-/-}$ and DIO *Psgl-1*$^{-/-}$ mice compared with *Psgl-1*$^{+/+}$ and DIO *Psgl-1*$^{+/+}$ mice (Fig. 1*A*). DIO did not affect the levels of MCP-1 in either group (Fig. 1*A*). Leptin levels were significantly increased in DIO *Psgl-1*$^{+/+}$ and DIO *Psgl-1*$^{-/-}$ mice compared with lean control groups (Fig. 1*A*). Other circulating inflammatory

TABLE 1
Metabolic parameters of control and DIO mice

	Control		DIO	
	Psgl-1$^{+/+}$	*Psgl-1*$^{-/-}$	*Psgl-1*$^{+/+}$	*Psgl-1*$^{-/-}$
Body weight (g)	28.6 ± 0.4	31.7 ± 3.0	44.6 ± 2.7*	43.8 ± 3.2†
Blood glucose (mg/dL)	110.9 ± 10.5	141.0 ± 21.9	270.2 ± 15.9*	222.7 ± 14.7*
Plasma insulin (ng/mL)	1.57 ± 0.3	1.13 ± 0.4	2.15 ± 0.3	2.0 ± 0.4
HOMA-IR	0.47 ± 0.1	0.38 ± 0.1	5.85 ± 2.6*	1.0 ± 0.2
Plasma FFA (mEq/L)	0.75 ± 0.1	0.71 ± 0.1	1.29 ± 0.1‡	0.86 ± 0.1
Plasma adiponectin (μg/mL)	34.75 ± 5.9	33.64 ± 6.6	36.16 ± 6.7	35.69 ± 3.9
Gonadal fat (g)	0.39 ± 0.05	0.81 ± 0.23	2.30 ± 0.39*	2.38 ± 0.17*
Perivascular fat (g)	0.20 ± 0.02	0.25 ± 0.03	0.55 ± 0.06*	0.56 ± 0.05*
Systolic BP (mmHg)	121.0 ± 5.0	110.3 ± 7.5	112.0 ± 6.9	106.8 ± 2.5

*$P < 0.01$ compared with corresponding control. †$P < 0.05$ compared with corresponding control. ‡$P < 0.01$ compared with other groups.

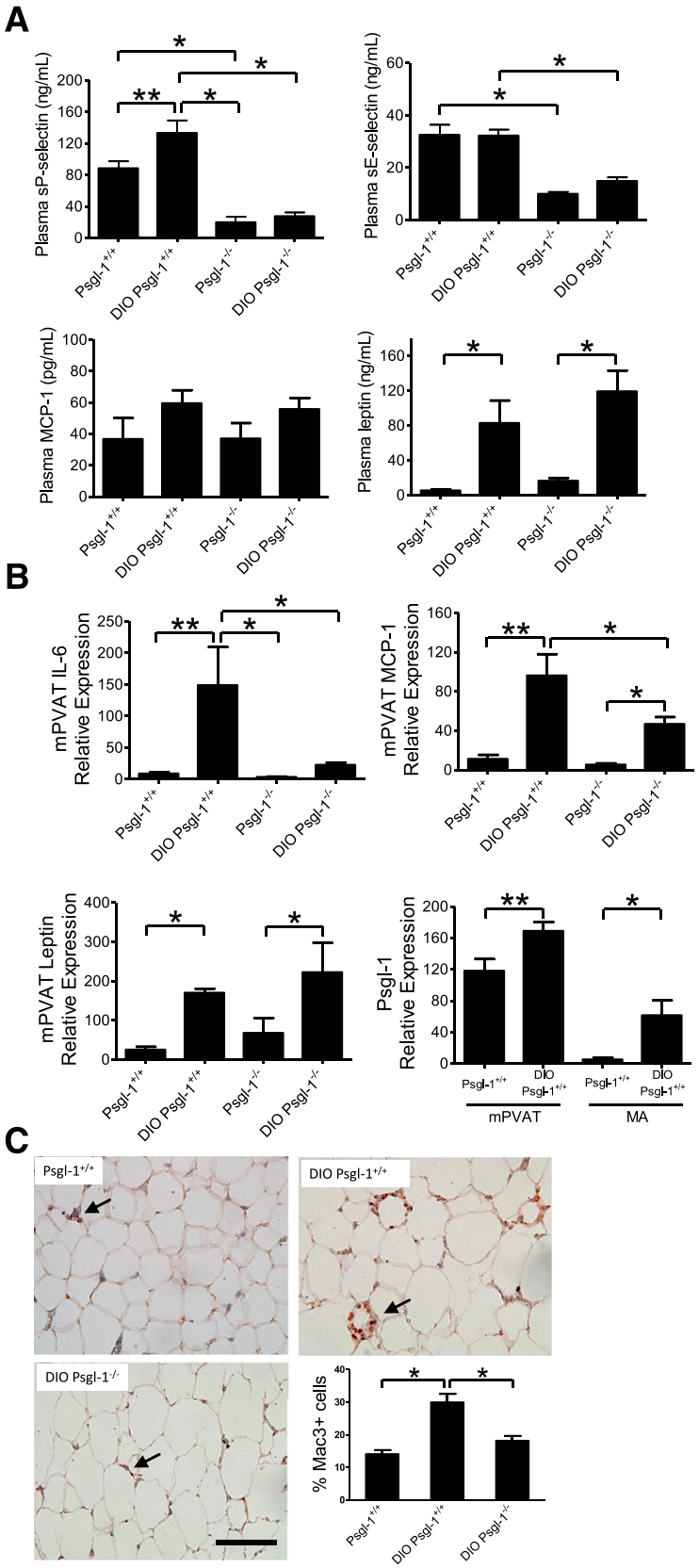

FIG. 1. Circulating levels, expression of biomarkers, and macrophage content in control and DIO mice (n = 6–8 per group). *A*: Circulating levels of sP-sel, sE-sel, MCP-1, and leptin. *B*: Expression of IL-6, MCP-1, leptin, and Psgl-1 in mPVAT and Psgl-1 in mesenteric arteries (MA). *C*: Macrophage content in mPVAT. Arrows: Mac-3–positive macrophages. Scale bar: 100 μm. *P < 0.01; **P < 0.05. (A high-quality color representation of this figure is available in the online issue.)

cytokines, including IL-1β, IL-6, and tumor necrosis factor-α (TNF-α), were tested but were below detection range.

Expression levels of IL-6, MCP-1, leptin, and Psgl-1. To characterize the effect of DIO on mPVAT, the mRNA expression levels of IL-6, MCP-1, leptin, and Psgl-1 were assessed using real-time PCR. The expression levels of IL-6 and MCP-1 were significantly increased in DIO *Psgl-1*$^{+/+}$ mice compared with standard chow–fed *Psgl-1*$^{+/+}$ mice and were significantly reduced in DIO *Psgl-1*$^{-/-}$ mice compared with DIO *Psgl-1*$^{+/+}$ mice (Fig. 1*B*). The leptin levels were significantly increased in DIO *Psgl-1*$^{+/+}$ and DIO *Psgl-1*$^{-/-}$ mice compared with control groups (Fig. 1*B*). The levels of Psgl-1 in mPVAT and mesenteric arteries were significantly higher in DIO *Psgl-1*$^{+/+}$ mice compared with standard chow–fed *Psgl-1*$^{+/+}$ mice (Fig. 1*B*).

Macrophage accumulation in perivascular adipose tissue. To determine the effect of DIO and Psgl-1 deficiency on perivascular adipose tissue inflammation, macrophages were quantitated from fat surrounding mesenteric arteries using Mac-3 immunostaining (Fig. 1*C*). The macrophage content of mPVAT was increased in DIO *Psgl-1*$^{+/+}$ mice compared with standard chow–fed *Psgl-1*$^{+/+}$ mice, but the mPVAT macrophage content was significantly reduced in DIO *Psgl-1*$^{-/-}$ mice compared with DIO *Psgl-1*$^{+/+}$ mice (Fig. 1*C*).

Vascular superoxide and nitrotyrosine in mesenteric arteries. As a measure of local oxidative stress, vascular superoxide was measured from cross-sections of mesenteric arteries using DHE staining (Fig. 2). Superoxide staining was significantly increased in mesenteric arteries of DIO *Psgl-1*$^{+/+}$ mice compared with standard chow–fed *Psgl-1*$^{+/+}$ mice; however, superoxide staining in DIO *Psgl-1*$^{-/-}$ mice was reduced compared with DIO *Psgl-1*$^{+/+}$ mice and was not different between standard chow–fed *Psgl-1*$^{+/+}$ or *Psgl-1*$^{-/-}$ mice.

Protein expression levels of nitrotyrosine were determined by immunoblotting. Nitrotyrosine protein expression in mesenteric arteries was increased in DIO *Psgl-1*$^{+/+}$ mice, but not in standard chow-fed *Psgl-1*$^{+/+}$ mice and DIO *Psgl-1*$^{-/-}$ mice (Fig. 2*F*).

Morphology and vascular function of mesenteric and carotid arteries. The morphologic properties of mesenteric arteries were characterized in Ca^{2+}-free conditions. No significant differences were detected in baseline lumen diameter, wall thickness, media-to-lumen ratio, and media cross-sectional area among the groups (Table 2).

NE-induced concentration-dependent contractile responses in mesenteric arteries were similar between *Psgl-1*$^{+/+}$ mice and *Psgl-1*$^{-/-}$ mice fed both standard chow and HFD (Fig. 3*A*). Endothelium-independent vasorelaxation responses to SNP were also similar between the groups (Fig. 3*B*). Endothelial-dependent vasorelaxation was evaluated with Ach. Vasorelaxation responses to Ach were significantly reduced in DIO *Psgl-1*$^{+/+}$ mice compared with standard chow–fed *Psgl-1*$^{+/+}$ mice; however, DIO *Psgl-1*$^{-/-}$ mice were protected against endothelial dysfunction with responses similar to standard chow–fed *Psgl-1*$^{+/+}$ and *Psgl-1*$^{-/-}$ mice (Fig. 3*C*). Ach-induced vasorelaxation was inhibited in all groups after preincubation with L-NAME (Fig. 3*D*). The bioavailability of NO was determined by differences in Ach-induced maximal vasorelaxation in the presence and absence of L-NAME. NO-mediated relaxation was significantly reduced in DIO *Psgl-1*$^{+/+}$ mice compared with standard chow–fed *Psgl-1*$^{+/+}$ mice, whereas

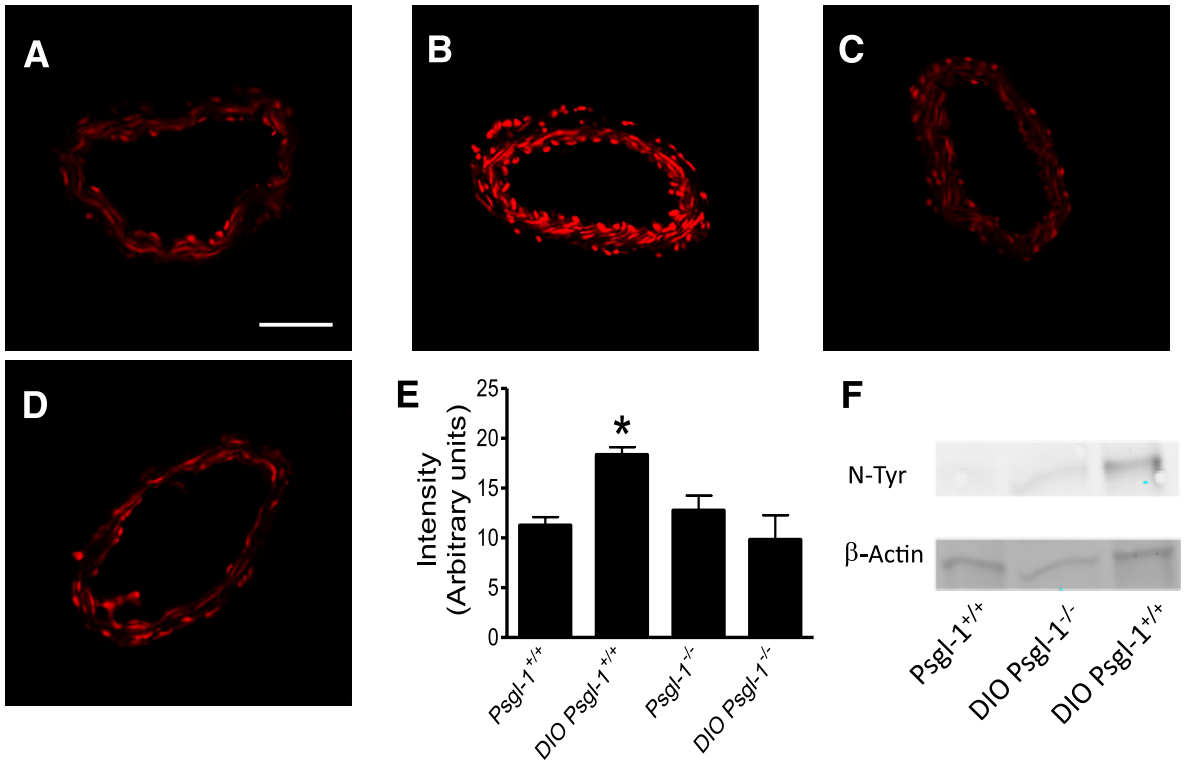

FIG. 2. Vascular superoxide detection by DHE fluorescence and nitrotyrosine by immunoblotting. Representative sections of confocal micrographs of sections of mesenteric arteries from control *Psgl-1*$^{+/+}$ (*A*), DIO *Psgl-1*$^{+/+}$ (*B*), control *Psgl-1*$^{-/-}$ (*C*), and DIO *Psgl-1*$^{-/-}$ mice (*D*). *E*: Pooled data of DHE fluorescence. *F*: Nitrotyrosine (*N*-Tyr) content in mesenteric arteries. Scale bar: 50 μm. $n = 5$ per group, *$P < 0.05$ compared with DIO *Psgl-1*$^{-/-}$ mice, control *Psgl-1*$^{+/+}$, and control *Psgl-1*$^{-/-}$ mice. (A high-quality color representation of this figure is available in the online issue.)

TABLE 2
Morphologic properties of mesenteric arteries

	Control		DIO	
	Psgl-1$^{+/+}$	*Psgl-1*$^{-/-}$	*Psgl-1*$^{+/+}$	*Psgl-1*$^{-/-}$
Wall thickness (μm)	16.8 ± 1.3	17.6 ± 0.9	19.0 ± 0.9	17.8 ± 0.9
Lumen diameter (μm)	186.2 ± 18.1	194.5 ± 9.2	174.6 ± 7.6	188.6 ± 11.1
Media-to-lumen ratio (%)	19.6 ± 3.4	18.4 ± 1.8	22.2 ± 1.7	19.0 ± 0.9
Media cross-sectional area ($10^3\times$ μm^2)	10.6 ± 0.9	11.6 ± 0.4	11.5 ± 0.5	11.6 ± 1.2

NO-mediated relaxation in DIO *Psgl-1*$^{-/-}$ mice was not significantly different than in standard chow–fed *Psgl-1*$^{-/-}$ or *Psgl-1*$^{+/+}$ mice (Fig. 3*E*).

To determine the role of superoxide in mediating endothelial dysfunction induced by DIO, vessels were incubated with the superoxide scavenger, TEMPOL, for 30 min. Ach-induced vasorelaxation was significantly improved by TEMPOL in DIO *Psgl-1*$^{+/+}$ mice compared with vessels without TEMPOL treatment (Fig. 3*F*). Endothelium-independent vasorelaxation responses to SNP were similar between the groups after TEMPOL treatment (Fig. 3*G*). After treatment of TEMPOL, superoxide staining by DHE in vessels of DIO *Psgl-1*$^{+/+}$ mice was reduced compared with vessels without TEMPOL treatment (Fig. 3*H*).

To assess the potential effect of systemic inflammation induced by DIO on carotid arteries, the pressure myograph was used to test vascular function on carotid arteries from standard chow–fed and DIO *Psgl-1*$^{+/+}$ mice. Phenylephrine-induced concentration-dependent contractile responses (Fig. 4*A*), and Ach-induced concentration-dependent relaxation responses (Fig. 4*B*) were similar between the groups.

Direct local effect of mPVAT on vascular function. To determine the local effect of mPVAT on vascular function, the mesenteric arteries from standard chow–fed *Psgl-1*$^{+/+}$ mice were incubated in mPVAT from DIO *Psgl-1*$^{+/+}$ mice or DIO *Psgl-1*$^{-/-}$ mice in vitro. After incubation in mPVAT from DIO *Psgl-1*$^{+/+}$ mice, the endothelial-dependent vasorelaxation responses to Ach were significantly impaired compared with responses after incubation in mPVAT from DIO *Psgl-1*$^{-/-}$ mice (Fig. 5*B*). Ach-induced vasorelaxation was inhibited in both groups after preincubation with L-NAME (Fig. 5*C*). Vasoconstriction responses to NE and endothelial-independent vasorelaxation responses to SNP were similar between the groups (Fig. 5*A* and *D*).

Psgl-1 neutralization is protective against obesity-induced macrophage accumulation in perivascular adipose tissue and endothelial dysfunction. To test the potential therapeutic strategy of Psgl-1 blockade, 5 weekly injections of a Psgl-1–blocking antibody or control isotype were given to DIO *Psgl-1*$^{+/+}$ mice. After this regimen, the macrophage content of mPVAT was significantly reduced in DIO *Psgl-1*$^{+/+}$ mice that received the antibody compared with control isotype-injected DIO *Psgl-1*$^{+/+}$ mice (Fig. 6*D*). This reduced perivascular adipose tissue macrophage content did not affect NE-induced vasoconstriction responses (Fig. 6*A*) but did improve Ach-induced vasorelaxation (Fig. 6*B*). The endothelial-independent responses to SNP were similar between the groups (Fig. 6*C*).

DISCUSSION

Obesity is an inflammatory disease (11) and a risk factor for cardiovascular diseases (12,13). One of the earliest detectable vascular abnormalities associated with obesity is impaired vascular relaxation (4). Impaired vascular function has been shown to be predictive of later cardiovascular complications (14). This early endothelial dysfunction is associated with circulating markers of inflammation, suggesting interplay between leukocyte activity and endothelial properties (15). Currently, weight loss and physical activity are the most effective means to prevent or reduce these vascular abnormalities (16); however, sustained weight loss is difficult to achieve, so treatments designed to prevent the vascular effects of obesity are needed.

One of the mechanisms responsible for endothelial dysfunction in obesity may be accumulation of perivascular fat (17). Epicardial fat that overlays the heart and coronary arteries, as well as perivascular fat surrounding large arteries, are associated with vascular lesions (18–20) and may be causally related to local and systemic atherosclerosis. For example, transplantation of visceral fat to carotid arteries of atherosclerotic-prone mice triggered formation of a local atherosclerotic lesion, whereas transplantation of subcutaneous fat did not (21). An interaction between the visceral or perivascular adipocyte and infiltrating macrophages may be contributing to the adverse vascular effects of excess visceral adiposity.

Adipose tissue macrophage content increases in obesity, and this corresponds to increased expression of adipose tissue-related inflammatory cytokines (11). Inflammatory adipose tissue is preceded by increased leukocyte-endothelial interactions within the visceral fat depots (8,22). Adhesion molecules, including selectins, were upregulated in obese adipose tissue and participated in leukocyte recruitment (22). Mice deficient in Psgl-1 had reduced visceral adipose tissue macrophage content in the setting of obesity (8). Leukocyte Psgl-1 deficiency may therefore protect against the adverse vascular consequences of excess visceral adiposity.

Because endothelial dysfunction represents an early manifestation of vascular disease, we tested whether Psgl-1 deficiency would be protective against endothelial dysfunction in the setting of obesity. In this research, we studied mesenteric arteries because they are particularly amenable to analyses with arterial pressure myography. These arteries also become surrounded by visceral adipose tissue in the setting of obesity and are prone to atherosclerosis (23). This model thus allows us to study inflammatory characteristics of endogenous visceral adipose tissue and endothelial function involving adjacent arteries.

We used a 10-week DIO protocol because mice gain considerable weight and develop clear evidence of adipose tissue inflammation at this time point (8). Compared with lean mice, DIO mice in this study developed marked impairment of endothelial function. To perform this measure,

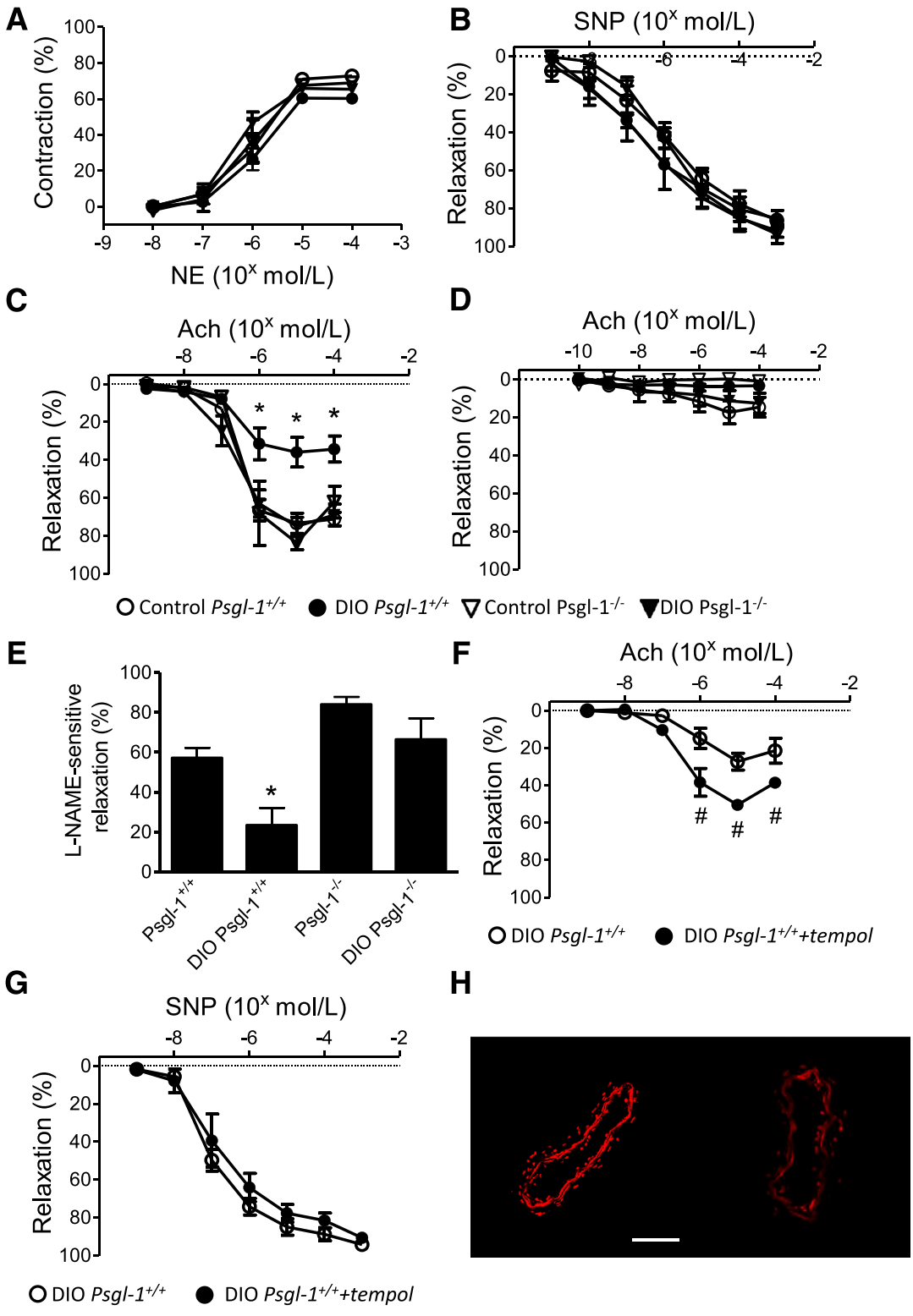

FIG. 3. Vasoconstriction and vasorelaxation responses of mesenteric arteries (MA) and DHE fluorescence of MA after treatment with TEMPOL. Control, DIO *Psgl-1*$^{+/+}$, and *Psgl-1*$^{-/-}$ mice (n = 5–7 per group). *A*: Concentration response to NE. *B*: Concentration response to SNP. *C*: Concentration response to Ach. *D*: Concentration response to Ach after preincubation in L-NAME. *E*: L-NAME–sensitive maximal vasorelaxation responses to Ach. *F*: Concentration response to Ach of MA from DIO *Psgl-1*$^{+/+}$ after treatment with TEMPOL. *G*: Concentration response to SNP of MA from DIO *Psgl-1*$^{+/+}$ after treatment with TEMPOL. *H*: DHE fluorescence of MA from DIO *Psgl-1*$^{+/+}$ without (*left*) and with (*right*) TEMPOL treatment. Scale bar: 50 μm. *P < 0.05 compared with DIO *Psgl-1*$^{-/-}$ mice, control *Psgl-1*$^{-/-}$ mice, and control *Psgl-1*$^{+/+}$ mice. #P < 0.05 compared with vessels without TEMPOL treatment. (A high-quality color representation of this figure is available in the online issue.)

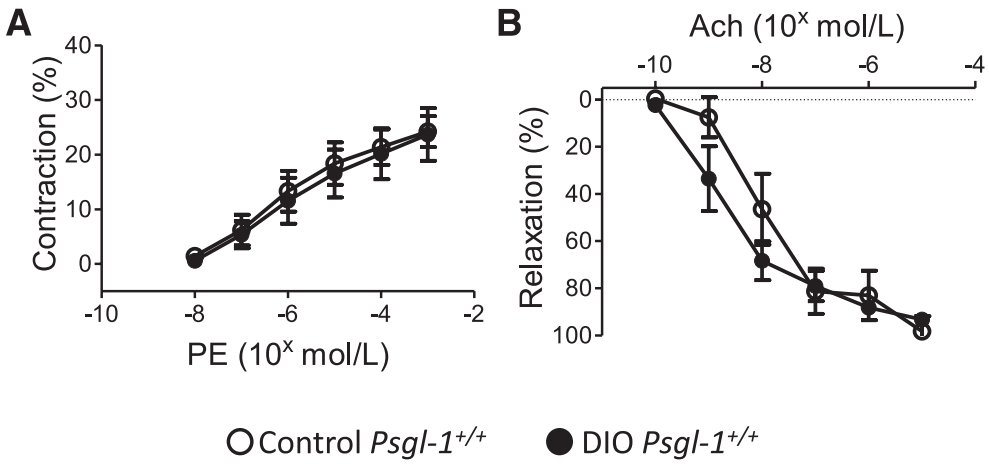

FIG. 4. Vasoconstriction and vasorelaxation responses of carotid arteries from control *Psgl-1*$^{+/+}$ and DIO *Psgl-1*$^{+/+}$ mice (n = 4 per group). *A*: Concentration response to phenylephrine (PE). *B*: Concentration response to Ach.

it was necessary to clear the tissue surrounding the vessel, including the adipose tissue. Thus, the dysfunction observed does not require the immediate presence of the perivascular adipose tissue and likely reflects a chronic effect of the adipose tissue on the endothelium. Anatomic measurements of the mesenteric arteries harvested from the obese and lean mice were similar; however, more macrophages were present in the perivascular adipose tissue and adjacent arteries from the DIO mice. This was associated with increased vascular superoxide and nitrotyrosine protein expression supporting the hypothesis that local excessive oxidative stress in the vessel wall leads to reduced endothelial NO bioavailability. The current study showed that the expression levels of inflammatory biomarkers are significantly elevated in mesenteric perivascular fat from DIO *Psgl-1*$^{+/+}$ mice. The carotid arteries,

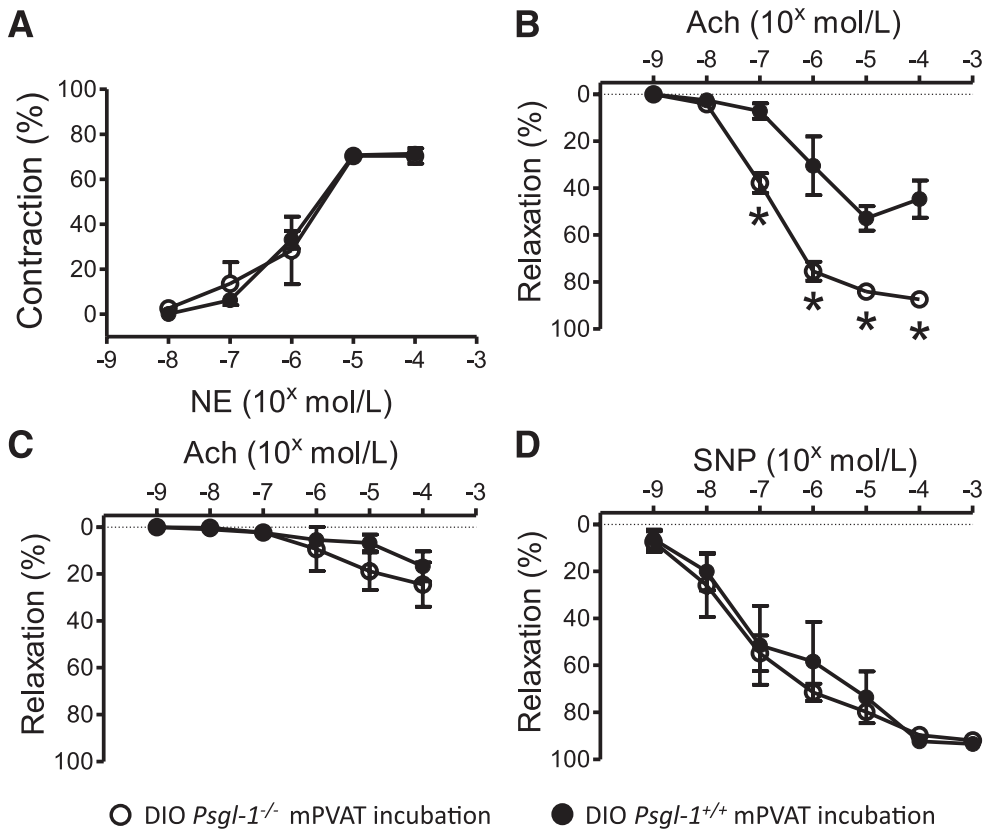

FIG. 5. Vasoconstriction and vasorelaxation responses of mesenteric arteries (MA) from standard chow–fed *Psgl-1*$^{+/+}$ mice after incubation in mPVAT from DIO *Psgl-1*$^{+/+}$ mice or DIO *Psgl-1*$^{-/-}$ mice. *A*: Concentration response to NE. *B*: Concentration response to Ach. *C*: Concentration response to Ach after preincubation in L-NAME. *D*: Concentration response to SNP. *P < 0.01 compared with MA incubated in mPVAT from DIO *Psgl-1*$^{+/+}$ mice.

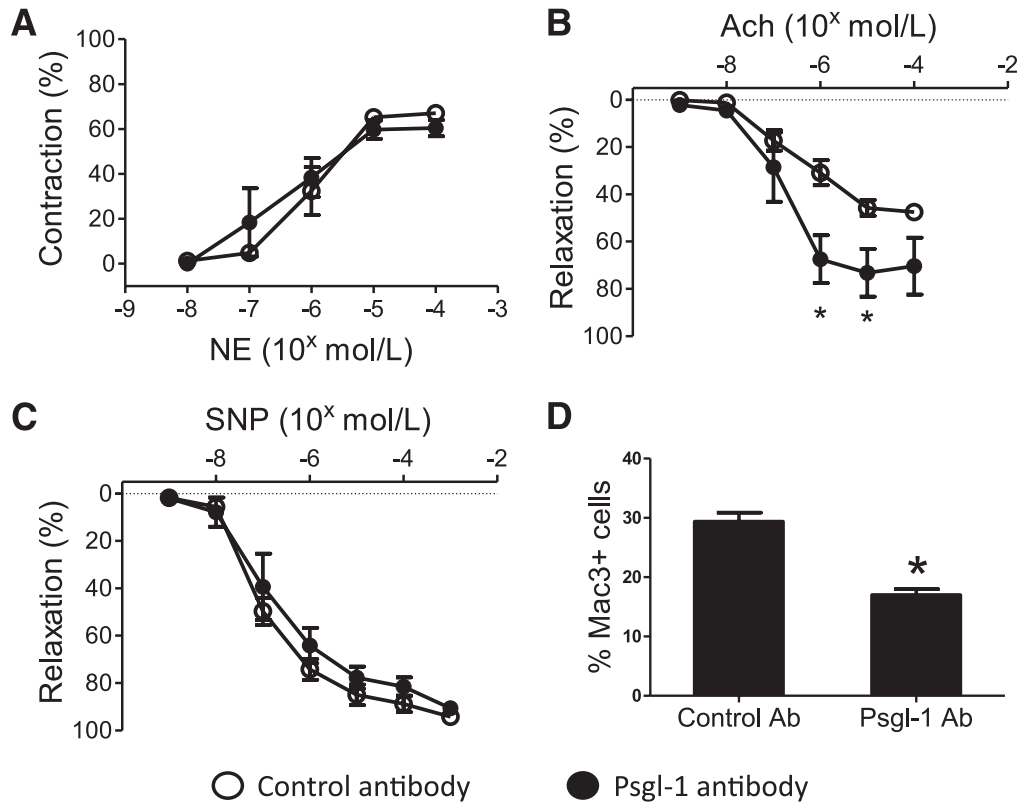

FIG. 6. Vasoactive responses of mesenteric arteries and macrophage content in mPVAT after anti–Psgl-1 treatment. DIO *Psgl-1*$^{+/+}$ after 5 weekly injections of control antibody or Psgl-1 antibody (n = 4 per group). *A*: Concentration response to NE. *B*: Concentration response to Ach. *C*: Concentration response to SNP. *D*: Macrophage content in mPVAT. *$P < 0.05$ compared with control antibody-injected DIO *Psgl-1*$^{+/+}$ mice.

which lack robust perivascular fat pads, did not show endothelial dysfunction, suggesting that local perivascular fat from DIO mice contributes more to vascular dysfunction than systemic effects in obesity.

Because we have previously shown that Psgl-1 deficiency leads to reduced adipose tissue inflammation in the setting of obesity (8) we tested the effect of Psgl-1 deficiency on endothelial dysfunction induced by obesity. As expected, Psgl-1 deficiency in DIO mice led to reduced accumulation of macrophages within the perivascular mesenteric adipose tissue. This was associated with reduced vessel wall superoxide content and nitrotyrosine. Previous research has demonstrated that excessive reactive oxygen species (ROS) are important in vascular dysfunction in different animal models of metabolic syndrome (24–26), and ROS are produced by multiple cell types, including endothelial cells, smooth muscle cells, and infiltrating inflammatory cells in the vasculature (25). NADPH oxidases and the mitochondria respiratory chain are major source of ROS in the vasculature (26,27).

The responsible cellular and enzymatic source of vascular superoxide in our study remains to be determined. The vessel wall superoxide appeared to be causally related to the endothelial dysfunction because the obesity-induced endothelial dysfunction was improved after treatment with the superoxide scavenger, TEMPOL. However, because TEMPOL only partially recovered endothelial dysfunction induced by the HFD, other factors may contribute to reduced NO bioavailability. Future in vivo experiments with TEMPOL or other antioxidants might be useful to reveal the relative importance of this mechanism.

Importantly, Psgl-1 deficiency prevented the endothelial dysfunction induced by DIO, presumably due to reduced perivascular adipose tissue inflammation and vessel wall oxidative stress. A supernatant prepared from obese homogenized fat was sufficient to induce endothelial dysfunction, and this effect was not present when the supernatant was prepared from obese Psgl-1–deficient fat. Although this fat supernatant experiment may not be reflective of the in vivo setting, because cells are homogenized, it supports the concept that an inflammatory factor derived from fat triggers local endothelial dysfunction and that this is reduced in the setting of Psgl-1 deficiency. Previous research reported that supernatants from inflammatory fat showed strong chemoattractant effects on leukocytes in vitro (28) and that several fat-derived inflammatory cytokines, such as IL-1β, IL-6, and TNF-α, are associated with increased NADPH oxidase expression and endothelial dysfunction (27,29–31). Identification of the specific downstream factor responsible for the Psgl-1 effect in our model will require further studies.

To determine whether Psgl-1 inhibition might be effective therapy for endothelial dysfunction associated with obesity, DIO *Psgl-1*$^{+/+}$ mice were treated with weekly injections of an antibody that blocks interactions between selectins and Psgl-1. Antibody injections were initiated at week 5, in the middle of the 10-week DIO protocol, to determine if Psgl-1 could prevent endothelial dysfunction while mice were in the process of gaining weight. Psgl-1 blockade in this setting was effective in reducing adipose tissue inflammation, endothelial dysfunction, and vascular superoxide production.

In the present study, we found that the HOMA-IR index was significantly increased in DIO *Psgl-1*$^{+/+}$ mice compared with lean control mice, as expected. In DIO *Psgl-1*$^{-/-}$ mice, HOMA-IR showed a trend toward protection, although it was not significant compared with DIO *Psgl-1*$^{+/+}$ mice. FFA levels were also significantly decreased in DIO *Psgl-1*$^{-/-}$ mice compared with DIO *Psgl-1*$^{+/+}$ mice, suggesting that Psgl-1 deficiency may correct other metabolic abnormalities in the setting of obesity. The underlying mechanisms responsible for this effect will also require additional study.

In conclusion, Psgl-1 deficiency is protective against obesity-induced endothelial dysfunction. Therapies designed to inhibit Psgl-1 binding to selectins may be useful to reduce preclinical vascular abnormalities associated with obesity.

ACKNOWLEDGMENTS

This work was supported by National Institutes of Health grants HL-57346 and HL-073150 to D.T.E. and by a Veterans Health Administration (VA) Merit Award (BX000353) to D.T.E.

No potential conflicts of interest relevant to this article were reported.

H.W. contributed to data acquisition and analysis and to writing the manuscript. W.L., J.W., C.G., X.W., S.L.W., and P.F.B., contributed to data acquisition. D.T.E. contributed to study conception and design and to manuscript revision and final approval of submitted version. D.T.E. is the guarantor of this work, and, as such, had full access to all the data in the study, and takes responsibility for the integrity of data and the accuracy of the data analysis.

The authors thank Dr. Y. Eugene Chen, University of Michigan, for assistance with BP measurements.

REFERENCES

1. Grundy SM. Obesity, metabolic syndrome, and cardiovascular disease. J Clin Endocrinol Metab 2004;89:2595–2600
2. Jiao P, Chen Q, Shah S, et al. Obesity-related upregulation of monocyte chemotactic factors in adipocytes: involvement of nuclear factor-kappaB and c-Jun NH2-terminal kinase pathways. Diabetes 2009;58:104–115
3. Weisberg SP, McCann D, Desai M, Rosenbaum M, Leibel RL, Ferrante AW Jr. Obesity is associated with macrophage accumulation in adipose tissue. J Clin Invest 2003;112:1796–1808
4. Bhattacharjee R, Alotaibi WH, Kheirandish-Gozal L, Capdevila OS, Gozal D. Endothelial dysfunction in obese non-hypertensive children without evidence of sleep disordered breathing. BMC Pediatr 2010;10:8
5. Valle Jiménez M, Estepa RM, Camacho RM, Estrada RC, Luna FG, Guitarte FB. Endothelial dysfunction is related to insulin resistance and inflammatory biomarker levels in obese prepubertal children. Eur J Endocrinol 2007;156:497–502
6. Endemann DH, Schiffrin EL. Endothelial dysfunction. J Am Soc Nephrol 2004;15:1983–1992
7. Hidalgo A, Peired AJ, Wild MK, Vestweber D, Frenette PS. Complete identification of E-selectin ligands on neutrophils reveals distinct functions of PSGL-1, ESL-1, and CD44. Immunity 2007;26:477–489
8. Russo HM, Wickenheiser KJ, Luo W, et al. P-selectin glycoprotein ligand-1 regulates adhesive properties of the endothelium and leukocyte trafficking into adipose tissue. Circ Res 2010;107:388–397
9. Matthews DR, Hosker JP, Rudenski AS, Naylor BA, Treacher DF, Turner RC. Homeostasis model assessment: insulin resistance and beta-cell function from fasting plasma glucose and insulin concentrations in man. Diabetologia 1985;28:412–419
10. Livak KJ, Schmittgen TD. Analysis of relative gene expression data using real-time quantitative PCR and the 2(-Delta Delta C(T)) Method. Methods 2001;25:402–408
11. Wellen KE, Hotamisligil GS. Obesity-induced inflammatory changes in adipose tissue. J Clin Invest 2003;112:1785–1788
12. Stevens J, Cai J, Pamuk ER, Williamson DF, Thun MJ, Wood JL. The effect of age on the association between body-mass index and mortality. N Engl J Med 1998;338:1–7
13. Wilson PW, D'Agostino RB, Sullivan L, Parise H, Kannel WB. Overweight and obesity as determinants of cardiovascular risk: the Framingham experience. Arch Intern Med 2002;162:1867–1872
14. Aggoun Y, Farpour-Lambert NJ, Marchand LM, Golay E, Maggio AB, Beghetti M. Impaired endothelial and smooth muscle functions and arterial stiffness appear before puberty in obese children and are associated with elevated ambulatory blood pressure. Eur Heart J 2008;29:792–799
15. Bhattacharjee R, Kim J, Alotaibi WH, Kheirandish-Gozal L, Capdevila OS, Gozal D. Endothelial dysfunction in non-hypertensive children: potential contributions of obesity and obstructive sleep apnea. Chest 2012;141:682–691
16. Farpour-Lambert NJ, Aggoun Y, Marchand LM, Martin XE, Herrmann FR, Beghetti M. Physical activity reduces systemic blood pressure and improves early markers of atherosclerosis in pre-pubertal obese children. J Am Coll Cardiol 2009;54:2396–2406
17. Ma L, Ma S, He H, et al. Perivascular fat-mediated vascular dysfunction and remodeling through the AMPK/mTOR pathway in high-fat diet-induced obese rats. Hypertens Res 2010;33:446–453
18. Konishi M, Sugiyama S, Sugamura K, et al. Association of pericardial fat accumulation rather than abdominal obesity with coronary atherosclerotic plaque formation in patients with suspected coronary artery disease. Atherosclerosis 2010;209:573–578
19. Alexopoulos N, McLean DS, Janik M, Arepalli CD, Stillman AE, Raggi P. Epicardial adipose tissue and coronary artery plaque characteristics. Atherosclerosis 2010;210:150–154
20. Ueno K, Anzai T, Jinzaki M, et al. Increased epicardial fat volume quantified by 64-multidetector computed tomography is associated with coronary atherosclerosis and totally occlusive lesions. Circ J 2009;73:1927–1933
21. Öhman MK, Luo W, Wang H, et al. Perivascular visceral adipose tissue induces atherosclerosis in apolipoprotein E deficient mice. Atherosclerosis 2011;219:33–39
22. Nishimura S, Manabe I, Nagasaki M, et al. In vivo imaging in mice reveals local cell dynamics and inflammation in obese adipose tissue. J Clin Invest 2008;118:710–721
23. Nakashima Y, Plump AS, Raines EW, Breslow JL, Ross R. ApoE-deficient mice develop lesions of all phases of atherosclerosis throughout the arterial tree. Arterioscler Thromb 1994;14:133–140
24. Bourgoin F, Bachelard H, Badeau M, et al. Endothelial and vascular dysfunctions and insulin resistance in rats fed a high-fat, high-sucrose diet. Am J Physiol Heart Circ Physiol 2008;295:H1044–H1055
25. Marchesi C, Ebrahimian T, Angulo O, Paradis P, Schiffrin EL. Endothelial nitric oxide synthase uncoupling and perivascular adipose oxidative stress and inflammation contribute to vascular dysfunction in a rodent model of metabolic syndrome. Hypertension 2009;54:1384–1392
26. Zhang H, Wang Y, Zhang J, Potter BJ, Sowers JR, Zhang C. Bariatric surgery reduces visceral adipose inflammation and improves endothelial function in type 2 diabetic mice. Arterioscler Thromb Vasc Biol 2011;31:2063–2069
27. Brandes RP, Kreuzer J. Vascular NADPH oxidases: molecular mechanisms of activation. Cardiovasc Res 2005;65:16–27
28. Henrichot E, Juge-Aubry CE, Pernin A, et al. Production of chemokines by perivascular adipose tissue: a role in the pathogenesis of atherosclerosis? Arterioscler Thromb Vasc Biol 2005;25:2594–2599
29. Martinez-Revelles S, Jiménez-Altayó F, Caracuel L, Pérez-Asensio FJ, Planas AM, Vila E. Endothelial dysfunction in rat mesenteric resistance artery after transient middle cerebral artery occlusion. J Pharmacol Exp Ther 2008;325:363–369
30. Jiang F, Lim HK, Morris MJ, et al. Systemic upregulation of NADPH oxidase in diet-induced obesity in rats. Redox Rep 2011;16:223–229
31. Chamberlain J, Francis S, Brookes Z, et al. Interleukin-1 regulates multiple atherogenic mechanisms in response to fat feeding. PLoS ONE 2009;4:e5073